

RESEARCH

Open Access



HMGB1 mediates synaptic loss and cognitive impairment in an animal model of sepsis-associated encephalopathy

Xiao-Yu Yin^{1†}, Xiao-Hui Tang^{2†}, Shi-Xu Wang¹, Yong-Chang Zhao¹, Min Jia², Jian-Jun Yang^{2*}, Mu-Huo Ji^{3*} and Jin-Chun Shen^{1*}

Abstract

Background Microglial activation-mediated neuroinflammation is one of the essential pathogenic mechanisms of sepsis-associated encephalopathy (SAE). Mounting evidence suggests that high mobility group box-1 protein (HMGB1) plays a pivotal role in neuroinflammation and SAE, yet the mechanism by which HMGB1 induces cognitive impairment in SAE remains unclear. Therefore, this study aimed to investigate the mechanism of HMGB1 underlying cognitive impairment in SAE.

Methods An SAE model was established by cecal ligation and puncture (CLP); animals in the sham group underwent cecum exposure alone without ligation and perforation. Mice in the inflachromene (ICM) group were continuously injected with ICM intraperitoneally at a daily dose of 10 mg/kg for 9 days starting 1 h before the CLP operation. The open field, novel object recognition, and Y maze tests were performed on days 14–18 after surgery to assess locomotor activity and cognitive function. HMGB1 secretion, the state of microglia, and neuronal activity were measured by immunofluorescence. Golgi staining was performed to detect changes in neuronal morphology and dendritic spine density. In vitro electrophysiology was performed to detect changes in long-term potentiation (LTP) in the CA1 of the hippocampus. In vivo electrophysiology was performed to detect the changes in neural oscillation of the hippocampus.

Results CLP-induced cognitive impairment was accompanied by increased HMGB1 secretion and microglial activation. The phagocytic capacity of microglia was enhanced, resulting in aberrant pruning of excitatory synapses in the hippocampus. The loss of excitatory synapses reduced neuronal activity, impaired LTP, and decreased theta oscillation in the hippocampus. Inhibiting HMGB1 secretion by ICM treatment reversed these changes.

Conclusions HMGB1 induces microglial activation, aberrant synaptic pruning, and neuron dysfunction in an animal model of SAE, leading to cognitive impairment. These results suggest that HMGB1 might be a target for SAE treatment.

[†]Xiao-Yu Yin and Xiao-Hui Tang contributed equally to this work

*Correspondence:

Jian-Jun Yang

yjyangjj@126.com

Mu-Huo Ji

jimuhuo2009@sina.com

Jin-Chun Shen

yshen0203@163.com

Full list of author information is available at the end of the article



Keywords Sepsis, High mobility group box-1 protein, Microglia, Synaptic pruning, Cognitive impairment

Introduction

Sepsis-associated encephalopathy (SAE) is a diffuse cerebral dysfunction caused by sepsis without direct central nervous system (CNS) infection or other types of encephalopathy [1]. SAE manifests as varying degrees of impaired consciousness, from mild delirium to coma, along with electroencephalographic (EEG) changes [2, 3], which severely reduces patients' quality of life, increases mortality rates, and places tremendous economic pressure on society, families, and individuals [4]. Previous studies have shown that SAE development may be related to neuroinflammation, blood–brain barrier (BBB) disruption, abnormal synaptic function, and mitochondrial dysfunction [5–7]; however, the exact mechanism remains unclear.

High mobility group box-1 protein (HMGB1) is a non-histone DNA binding protein present in the nucleus of eukaryotic cells. HMGB1 is released passively from damaged cells and is actively extracellularly secreted by activated immune cells [8]. When immune cells are exposed to microbe-associated molecular patterns, pathogen-associated molecular patterns, and endogenous inflammatory mediators, HMGB1 activates immune cells and mediates the inflammatory response [9]. One recent study demonstrated that pregabalin ameliorates microglial activation and neuronal damage by blocking the HMGB1 signaling pathway in radiation-induced brain injury [10]. HMGB1 is also involved in cognitive impairment-related diseases, such as Alzheimer's disease (AD) and traumatic brain injury (TBI) [11, 12]. Notably, HMGB1 is a late mediator of inflammation in sepsis [13]. In an animal model of SAE, the serum levels of HMGB1 are increased in sepsis survivors, which remains elevated for at least 4 weeks after CLP [14, 15]. Inflammation (ICM) is a small molecule that can block cytoplasmic localization and extracellular release of HMGBs by perturbing its post-translational modification [16]. ICM treatment inhibits the cytosolic translocation of HMGB1, which is confirmed by genetic experiments based on the silencing of HMGB1 [17]. A previous study also revealed that using ICM can inhibit HMGB1 release thus limiting fructose 1,6-bisphosphatase 1-dependent hepatic stellate cell activation, the development of the secretory phenotype and tumor progression [18]. However, the specific mechanism by which HMGB1 results in cognitive impairment in SAE remains unclear.

Microglia, the primary innate immune cell population in the brain, can actively release HMGB1. HMGB1 can bind to microglial surface receptors to activate

downstream inflammatory pathways and promote microglial activation [9]. Microglial activation plays essential roles in immune surveillance, synaptic plasticity regulation, and maintaining dynamic homeostasis within the CNS [19]. Microglia are activated under pathological conditions, inducing synaptic loss, neuron dysfunction, and neural circuit disruption [20, 21]. These abnormalities might contribute to the pathogenesis of cognitive impairment in many diseases. Therefore, we hypothesized that HMGB1 secretion mediates microglial activation, aberrant synaptic pruning, and neuronal dysfunction, ultimately leading to cognitive impairment in SAE mice.

Materials and method

Animals

C57BL/6JGpt male mice (10–12 weeks, 20–30 g) were provided by Jiangsu Jicui Pharmachem Biotechnology Co. All mice were housed under standard laboratory conditions with an automatically controlled temperature of 22 ± 2 °C, 55–65% humidity, and 12 h–12 h light–dark cycle. Four to 5 mice were housed per cage, with unlimited access to food and water.

SAE model

SAE was induced by cecal ligation and puncture (CLP). The mice were anesthetized by intraperitoneal injection of 1% pentobarbital sodium. A 1.5 cm midline incision was performed in the abdomen to expose the cecum. The exposed cecum was ligated with 4-0 sutures below the ileocecal valve (5 mm from the cecal tip). Then, a 22 G needle was used to puncture the cecum, and a small volume of feces was gently squeezed out. After the cecum was returned to the abdominal cavity, the abdomen was closed in sequence. The mice were resuscitated immediately by hypodermic injection of normal saline (20 ml/kg), placed on a heat blanket and returned to the original cage after awakening from anesthesia. The same incision was cut in the abdomen to expose the cecum in the sham group mice, and no ligation or perforation was performed.

Experimental design and drug treatment

Mice were randomly assigned to the sham + vehicle group (sham + vehicle), CLP + vehicle group (CLP + vehicle), sham + inflammation (ICM) group, or CLP + ICM group (CLP + ICM). ICM (Cayman, USA, 10 mg/kg) or vehicle (distilled water containing DMSO and PEG400) was administered intraperitoneally (*i.p.*)

daily for 9 consecutive days beginning 1 h before CLP operation [22]. The experimental protocol is presented in Fig. 1A.

Open field test

The open field test was performed to evaluate the locomotor activity of mice. A white open box (40 × 40 × 40 cm) divided into 16 squares was used. Each mouse was placed in the center of the box and allowed to

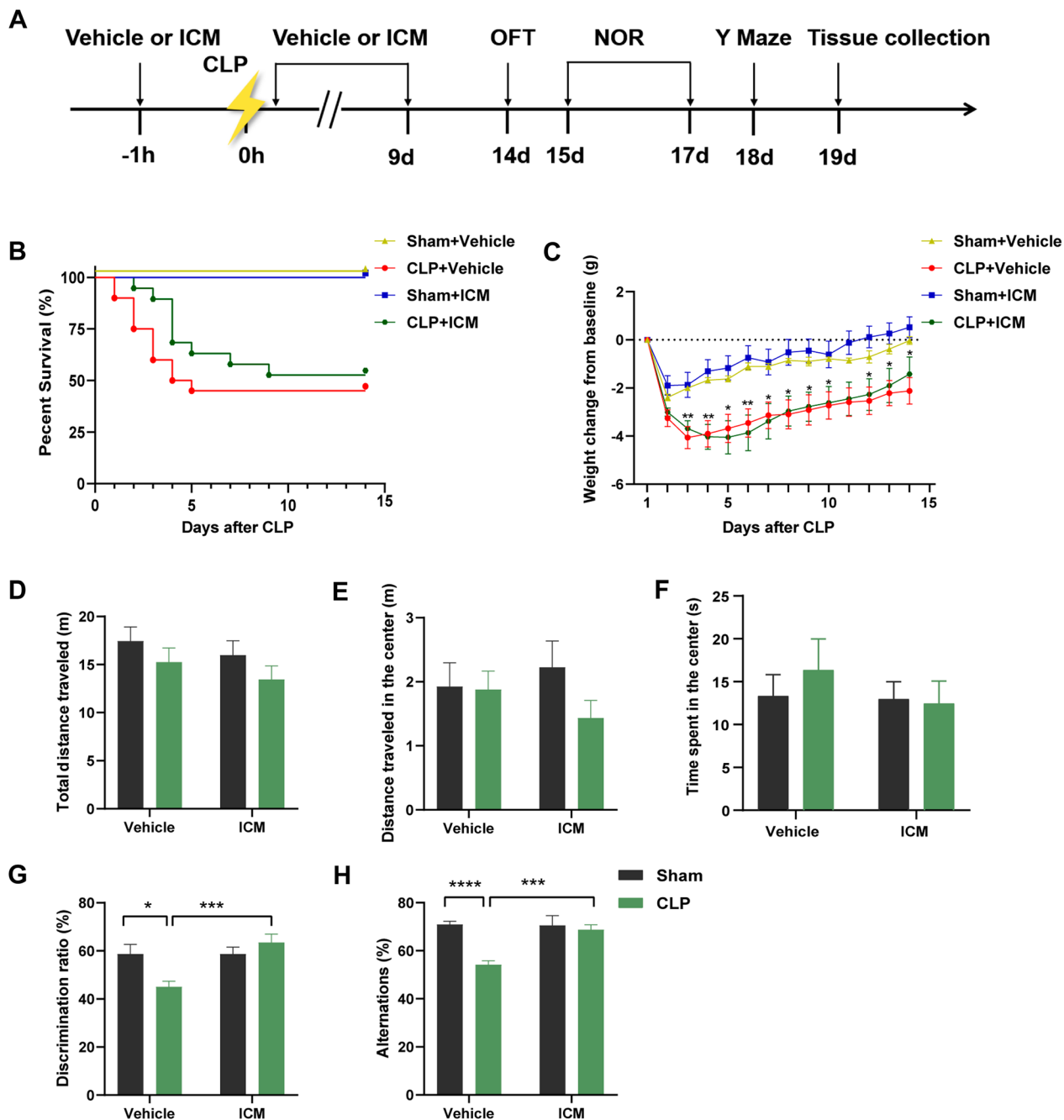


Fig. 1 ICM ameliorated sepsis-induced cognitive impairment. **A** Flow chart of the experiment. **B** Comparison of the mouse survival rates among the four groups. **C** Comparison of the mouse body weights among the four groups. **D–F** OFT performance among the four groups. **G** NOR performance among the four groups. **H** Y maze test performance among the four groups. Data are presented as the mean ± SEM (n = 8–12 mice per group). **P* < 0.05, ***P* < 0.01, ****P* < 0.001, *****P* < 0.0001 vs. the indicated groups

explore for 5 min freely. The total distance traveled in the arena was recorded. The chamber was cleaned with 75% ethanol between each trial.

Novel object recognition

New object recognition tests were carried out in a 40 × 40 × 40 cm white open box. The task procedure consists of the habituation, learning, and test phases. (1) In the habituation phase, mice were placed in the open box and allowed to explore freely for 10 min; (2) in the learning phase, after 1 day of habituation, mice were placed in the open box in the presence of two identical objects (A + A). (3) The test phase was conducted 24 h after the learning phase. One of the objects was replaced by a novel object, B, with a distinctively different color and shape. The length of time spent exploring familiar and novel objects was measured. The Discrimination Ratio was calculated as the new object exploration time/(new object exploration time + old object exploration time). The chamber and objects were cleaned with 75% ethanol between each trial.

Y maze

A Y maze test was conducted to measure spatial working memory. In this experiment, a Y-maze with three arms (A, B, and C) at a 120° angle was used. Each mouse was placed into the center of the maze at the beginning of the experiment and allowed to explore freely for 8 min. Spontaneous alternation was defined as three consecutive entries into different arms, e.g., ABC, BCA, and CAB. The percentage of spontaneous alternation was used to assess working memory ability. The percentage of spontaneous alternation was calculated as spontaneous alternation number/(total number of entries - 2) × 100%. Ethanol (75%) was used to clean the maze between each trial.

Immunofluorescence

Mice were deeply anesthetized by *i.p.* injection of 1% pentobarbital sodium and then transcardially perfused with ice-cold phosphate-buffered saline (PBS) followed by 4% paraformaldehyde (PFA). The brains were removed and postfixed in 4% PFA overnight and then dehydrated in 30% sucrose for 72 h at 4 °C. Brains were then sliced into 30 μm coronal sections and mounted on slides. Slices were permeabilized and blocked with PBS containing 0.3% Triton X-100 and 10% NDS for 1 h at room temperature. Primary antibodies were incubated in PBS containing 0.3% Triton X-100 and 5% NDS overnight [rabbit anti-Iba1, 1:500 (WAKO, cat#019-19741); goat anti-Iba1, 1:1000 (Abcam, ab5076); rabbit anti-HMGB1, 1:100 (Abcam, ab18256); rat anti-CD68, 1:500 (BioLegend, cat#137001); mouse anti-vglut1, 1:500 (SYSY,

135011) and rabbit anti-c-Fos, (CST, cat#2250)]. The brain sections were then washed with PBS and treated with appropriate secondary antibodies conjugated with Alexa Fluor fluorophore in PBS containing 0.3% Triton X-100 and 5% NDS for 1 h at room temperature. The sections were rewashed with PBS and counterstained with DAPI (1:1000; Beyotime Biotechnology) for nuclear staining. Slides were coverslipped with 50% glycerin. All images were acquired with Leica TCS SP5 and Zeiss LSM880 confocal microscopes.

Golgi staining

Golgi staining was performed per the Golgi staining kit (PK401, FD NeuroTechnologies) manufacturer's directions. Mice were anesthetized with 1% pentobarbital sodium intraperitoneally. Whole brains were dissected, immersed in solution A + B, and stored in the dark at room temperature. After 2 weeks, the brains were transferred to solution C for 3 days. One hundred millimeter-thick coronal slices were cut at room temperature with a Vibratome (Leica VT1000S) and transferred onto 1% gelatin-coated slides for staining. After staining with solution D + E + distillation-distillationH₂O and dehydration with different concentrations of ethanol series, the slices were cleared in xylene and coverslipped with neutral balsam mounting medium. All images were acquired with an Olympus BX53 microscope and analyzed with Fiji.

In vivo electrophysiology

The mice were anesthetized by intraperitoneal injection of 1% pentobarbital sodium and fixed on the stereotaxic apparatus after complete anesthesia. The bregma points were exposed by cutting the scalp and adjusting the plane on the axis of the front and rear fontanel line to make it on the same level. Two points on the left side of the skull were selected for the placement of cranial nails. A 2.5 × 2.5 mm bone window was made on the right skull surface, and the dura was carefully picked out with a syringe needle. An 8-channel microfilament electrode array was fixed on a brain stereotaxic instrument and slowly placed in the CA1 region of the hippocampus (anteroposterior: -2.2 mm, mediolateral: -1.5 mm, dorsoventral: -1.6 mm). The electrodes were fixed with bone cement after determining successful embedding. Raw data were recorded in NOR on day 14 after surgery. In our study, the bands were classified as delta oscillations (1–4 Hz), theta oscillations (4–8 Hz), alpha oscillations (8–12 Hz), beta oscillations (12–30 Hz), and gamma oscillations (30–90 Hz). The signals were filtered with a passband of 0.3–300 Hz and further amplified and digitized at 2 kHz. All data analyses were performed by Neuroexplorer (Plexon Corporation, Dallas, TX) software.

In vitro electrophysiology

After mice were anesthetized with isoflurane (5% air volume, 3 min), the whole brain was carefully removed and placed in 0 °C sucrose-rich artificial cerebrospinal fluid [ACSF; 126 NaCl, 2.5 KCl, 1 MgCl₂, 1 CaCl₂, 1.25 KH₂PO₄, 26 NaHCO₃, 20 glucose (mM)]. The brain was coronally cut out according to the brain atlas in 0 °C sucrose-rich ACSF with 95% O₂ and 5% CO₂ oxygenation conditions (thickness 250 μm, blade speed 0.14 mm/s). The hippocampal slices were transferred into ACSF with sufficient oxygenation and incubated at room temperature for at least 45 min to ensure complete cell activity recovery. The hippocampal slices were placed on a Nikon orthomosaic microscope (FN-1 with a 10 × 40 water immersion objective stage). The stimulating electrode was placed in the Schaffer collateral (SC) to deliver the test and conditioned stimulation. The recording electrode was placed 200–300 μm from the stimulation electrode in the stratum radiatum of CA1. Forty to 50% of the maximum EPSP value was used as the baseline. After 10 min of baseline stabilization, LTP was induced with three strings of high-frequency stimulation (HFS) (50 Hz, 100 pulse), and the slope of the potential was normalized to the mean base value. The data were recorded through a SutterPatch-IP2 amplifier, and data acquisition was performed by selecting signals in the range of 0–10 kHz and filtering them through a 5 kHz low-pass filter. Igor Pro9.0 was used to analyze the data [23].

Statistical analysis

GraphPad Prism 8.0 (GraphPad Software) was used for statistical analyses. Data are expressed as the mean ± standard error (mean ± SEM). The normality of data distribution was assessed by the Shapiro–Wilk test. When comparing multiple groups, data were analyzed using two-factor ANOVA followed by Tukey's post hoc test when appropriate. Changes in body weight from baseline were assessed using repeated-measures analysis of variance. Kaplan–Meier survival curves and log-rank analyses were used to compare survival outcomes between different groups. Statistical significance was defined at $P < 0.05$.

Results

ICM ameliorated sepsis-induced cognitive impairment

No mice in the sham + vehicle group died 14 days after surgery, while the 14-day survival rate after CLP was only 45% (Fig. 1B). The survival rate slightly increased after ICM administration, but there was no significant difference between the two groups (Fig. 1B). Postoperative body weight significantly decreased after CLP, but there was no significant difference between the CLP and

CLP + ICM groups (Fig. 1C). To assess locomotor activity and cognitive function, we performed OFT, Y maze, and NOR on days 14–18 after surgery. In the OFT, there was no significant difference in total distance traveled [Fig. 1D; interaction: CLP × ICM, $F(1, 36) = 0.01335$, $P = 0.9087$; CLP: $F(1, 36) = 1.206$, $P = 0.8753$; ICM: $F(1, 36) = 2.537$, $P = 0.9391$], distance traveled in the center [Fig. 1E; interaction: CLP × ICM, $F(1, 36) = 1.246$, $P = 0.2717$; CLP: $F(1, 36) = 0.04634$, $P = 0.9996$; ICM: $F(1, 36) = 1.584$, $P = 0.7558$], and time spent in the center [Fig. 1F; interaction: CLP × ICM, $F(1, 36) = 0.3539$, $P = 0.5556$; CLP: $F(1, 36) = 0.5084$, $P = 0.8833$; ICM: $F(1, 36) = 0.1762$, $P = 0.7657$] among the four groups (Fig. 1D, E). In the NOR test, the mice in the CLP + vehicle group spent less time with novel objects than those in the sham + vehicle group; this effect was reversed by ICM treatment [Fig. 1G; interaction: CLP × ICM, $F(1, 33) = 8.644$, $P = 0.0060$; CLP: $F(1, 33) = 8.767$, $P < 0.05$; ICM: $F(1, 33) = 1.981$, $P < 0.001$]. In the Y maze test, compared with the sham + vehicle group, the CLP + vehicle group showed a significant decrease in spontaneous alternation, and this effect was reversed by ICM treatment [Fig. 1H; interaction: CLP × ICM, $F(1, 38) = 10.61$, $P = 0.0024$; CLP: $F(1, 38) = 9.633$, $P < 0.0001$; ICM: $F(1, 38) = 16.25$, $P < 0.001$]. These results indicate that inhibiting HMGB1 rescues cognitive impairment in septic mice.

ICM ameliorated the abnormal secretion of HMGB1 in the hippocampus of SAE mice

We examined the expression of nuclear HMGB1 (n-HMGB1) in the hippocampus to reveal the underlying mechanism of SAE. Compared with the sham + vehicle group, the mean gray value of n-HMGB1 in microglia was significantly decreased in the CLP + vehicle group in the hippocampus, and this effect was reversed by ICM treatment [Fig. 2A, B; interaction: CLP × ICM, $F(1, 67) = 34.17$, $P < 0.0001$; CLP: $F(1, 67) = 20.24$, $P < 0.0001$; ICM: $F(1, 67) = 59.74$, $P < 0.0001$]. However, there were no significant differences in n-HMGB1 expression levels in non-microglia cells among the four groups [Fig. 2C; interaction: CLP × ICM, $F(1, 68) = 2.552$, $P = 0.1148$; CLP: $F(1, 68) = 3.991$, $P = 0.9504$; ICM: $F(1, 68) = 0.7091$, $P = 0.9920$]. These results suggest that HMGB1 secreted from microglia increases after CLP.

ICM restored the changes in the number and morphology of microglia in the hippocampus of SAE mice

The number of microglia was significantly increased in the CLP + vehicle group compared with the sham + vehicle group, and ICM treatment reversed this effect [Fig. 3A, B; interaction: CLP × ICM, $F(1, 60) = 0.3246$, $P = 0.5710$; CLP: $F(1, 60) = 41.44$, $P < 0.05$; ICM: $F(1, 60) = 13.71$, $P < 0.0001$]. The microglial morphological

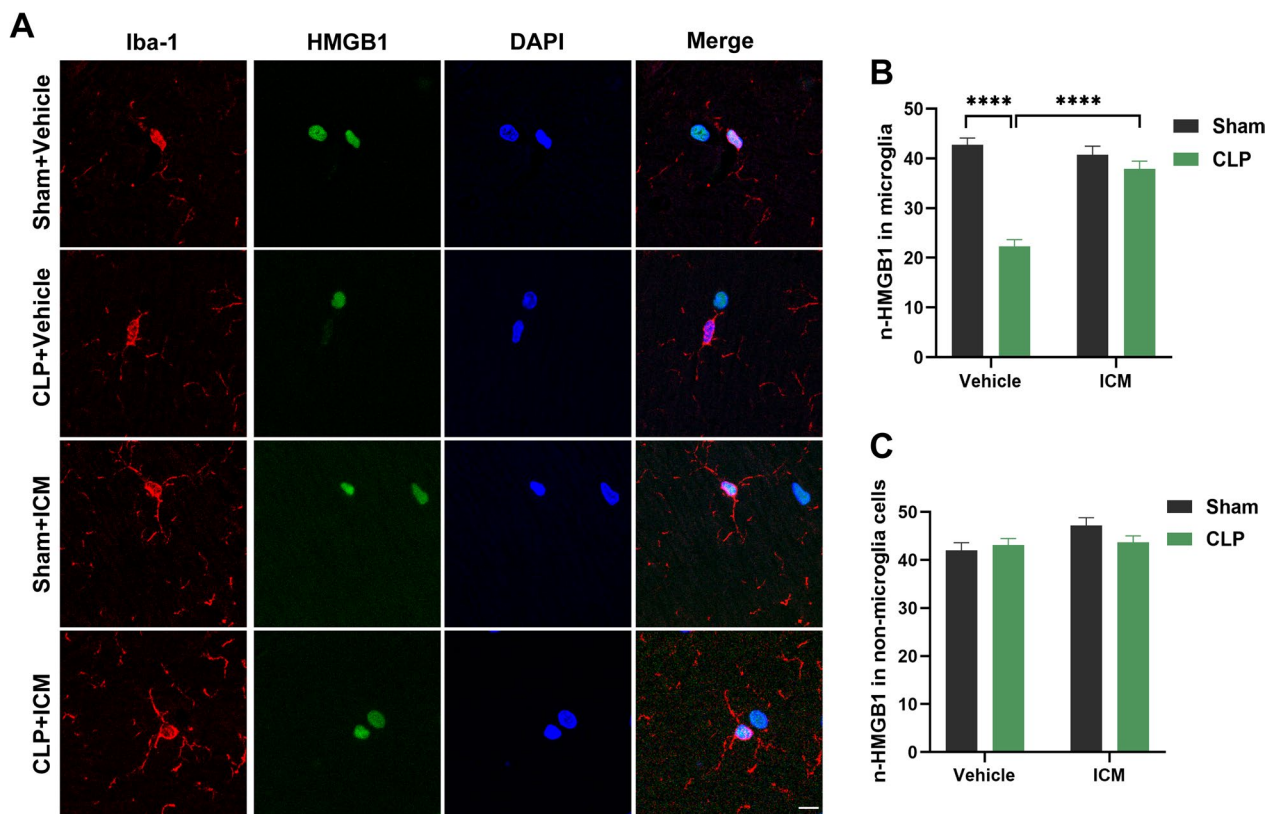


Fig. 2 ICM ameliorated the abnormal secretion of HMGB1 in the hippocampus of SAE mice. **A** Representative images of immunofluorescence staining of Iba-1 (red), HMGB1 (green), DAPI (blue) and colocalization in the hippocampus, scale bar = 10 μ m; **B, C** Quantification of the mean gray value of n-HMGB1 in microglia and non-microglia cells in the hippocampus among the four groups. Data are presented as the mean \pm SEM ($n = 3-4$ mice/group). **** $P < 0.0001$ vs. the indicated groups

analysis results showed that the average branch length and solidity of the microglia were significantly increased in the CLP + vehicle group compared to the sham + vehicle group; ICM treatment reversed this effect [Fig. 3C–E; D: interaction: CLP \times ICM, $F(1, 116) = 9.551$, $P = 0.0025$; CLP: $F(1, 116) = 14.96$, $P < 0.001$; ICM: $F(1, 116) = 10.36$, $P < 0.0001$; E: interaction: CLP \times ICM, $F(1, 68) = 19.25$, $P < 0.0001$; CLP: $F(1, 68) = 28.26$, $P < 0.0001$; ICM: $F(1, 68) = 49.09$, $P < 0.0001$]. The immunofluorescence results indicate that ICM reverses the microglial activation induced by CLP.

ICM reversed the enhanced phagocytic activity of microglia in the hippocampus of SAE mice

We measured microglial CD68 levels by immunofluorescence to further assess the changes in the phagocytic activity of microglia. The area percentage of CD68 expression in Iba1⁺ cells in the CLP + vehicle group was significantly increased compared with that in the sham + vehicle group, and this effect was reversed by ICM treatment [Fig. 4A, B; interaction: CLP \times ICM, $F(1, 184) = 22.61$, $P < 0.0001$; CLP: $F(1, 184) = 3.115$,

$P < 0.0001$; ICM: $F(1, 184) = 13.04$, $P < 0.0001$]. These data suggest that HMGB1 significantly increases microglial CD68 expression and provide evidence that HMGB1 may affect microglial phagocytic activity in SAE.

ICM reduced microglia-mediated synapse elimination in the hippocampus of SAE mice

We evaluated the area of engulfed VGLUT1⁺ puncta within Iba1⁺ cells by immunofluorescence to investigate whether HMGB1-induced microglial activation leads to synapse engulfment in SAE. The results showed that Iba1⁺ cells from the hippocampus of the CLP + vehicle group engulfed significantly more VGLUT1⁺ puncta than hippocampal Iba1⁺ cells from the sham + vehicle group, and this effect was reversed by ICM treatment [Fig. 5A, B; interaction: CLP \times ICM, $F(1, 116) = 9.551$, $P = 0.0025$; CLP: $F(1, 116) = 14.96$, $P < 0.001$; ICM: $F(1, 116) = 10.36$, $P < 0.0001$]. These data suggest that HMGB1 leads to aberrant pruning of hippocampal excitatory synapses through microglial activation.

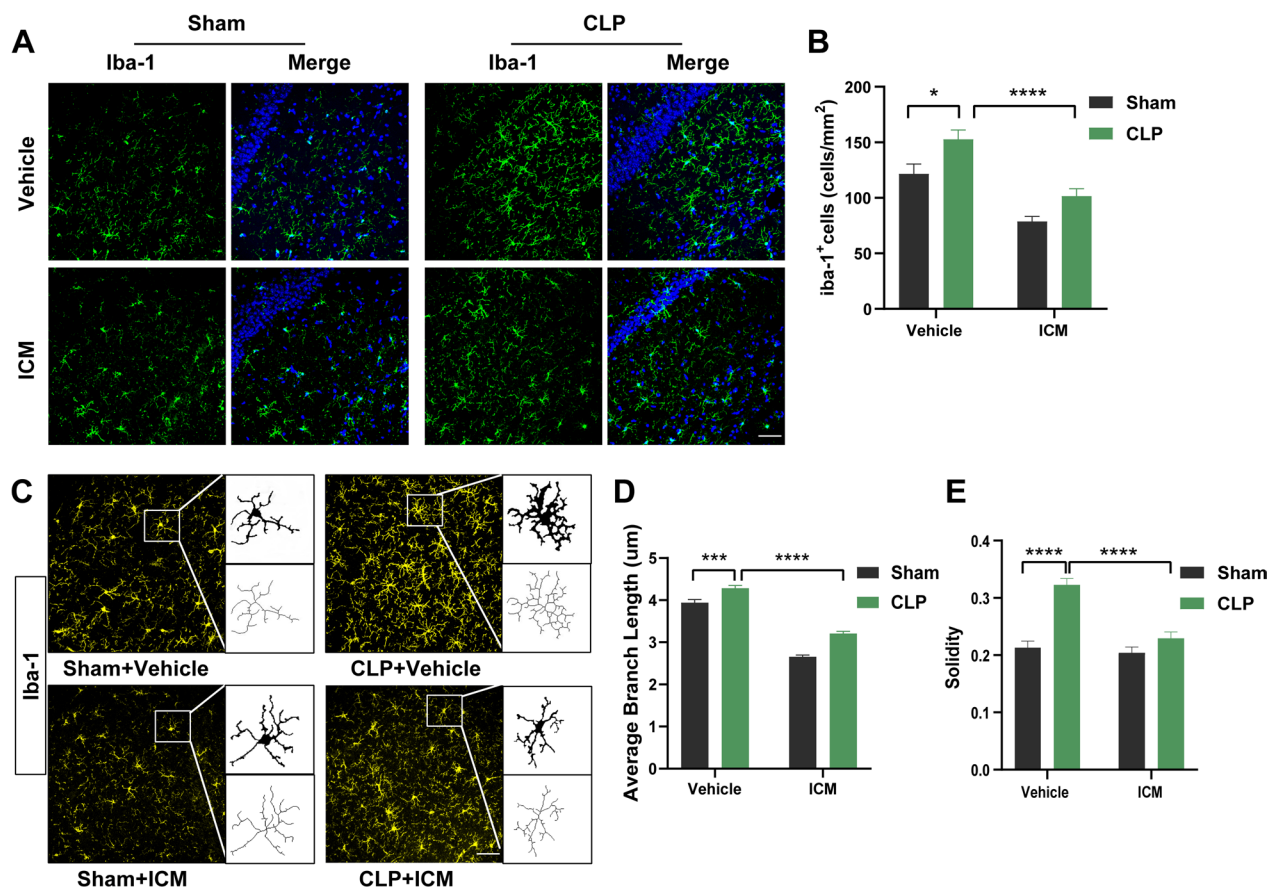


Fig. 3 ICM restored the changes in the number and morphology of microglia in the hippocampus of SAE mice. **A** Representative images of immunofluorescence staining of Iba-1 (green) and DAPI (blue) in the hippocampus, scale bar = 50 µm; **B** quantification of the number of Iba-1⁺ cells (microglia) in the hippocampus among the four groups; **C** representative images of immunofluorescence staining of Iba-1 (yellow) and skeletonization of Iba-1⁺ cells (microglia) in the hippocampus, scale bar = 50 µm; **D** quantification of the average branch length of Iba-1⁺ cells (microglia) in the hippocampus among the four groups; **E** quantification of the solidity of Iba-1⁺ cells (microglia) in the hippocampus among the four groups. Data are presented as the mean ± SEM (n = 3–5 mice/group). * $P < 0.05$, *** $P < 0.001$, **** $P < 0.0001$ vs. the indicated groups

ICM ameliorated abnormal neuronal morphology and loss of dendritic spines in the hippocampus of SAE mice

We next analyzed the morphology of Golgi-stained neurons and found that after CLP, the number of dendritic crossings of pyramidal neurons at 50 µm and 100 µm from the cell body was significantly reduced; ICM treatment reversed this effect [Fig. 6A, B; 50 µm: interaction: CLP × ICM, $F(1, 68) = 10.06$, $P = 0.0023$; CLP: $F(1, 68) = 32.60$, $P < 0.0001$; ICM: $F(1, 68) = 34.23$, $P < 0.0001$; 100 µm: interaction: CLP × ICM, $F(1, 68) = 1.950$, $P = 0.1671$; CLP: $F(1, 68) = 28.30$, $P < 0.0001$; ICM: $F(1, 68) = 35.03$, $P < 0.0001$]. Compared with the sham + vehicle group, the number of neuronal branches in the CA1 was significantly reduced in the CLP + vehicle group, and this effect was reversed by ICM treatment [Fig. 6C, D; interaction: CLP × ICM, $F(1, 68) = 13.38$, $P = 0.0005$; CLP:

$F(1, 68) = 32.02$, $P < 0.0001$; ICM: $F(1, 68) = 75.39$, $P < 0.0001$]. Compared with the sham + vehicle group, the total length of neuronal branches in the CA1 in the CLP + vehicle group was significantly reduced, and ICM treatment reversed this effect [Fig. 6E; interaction: CLP × ICM, $F(1, 68) = 20.44$, $P < 0.0001$; CLP: $F(1, 68) = 60.92$, $P < 0.0001$; ICM: $F(1, 68) = 76.45$, $P < 0.0001$]. An analysis of dendritic spine density in the CA1 by Golgi staining revealed that the dendritic spine density of pyramidal neurons in the CA1 of the hippocampus was significantly reduced in the CLP + vehicle group compared with the sham + vehicle group, and ICM treatment reversed this effect [Fig. 6F, G; interaction: CLP × ICM, $F(1, 68) = 42.89$, $P < 0.0001$; CLP: $F(1, 68) = 72.26$, $P < 0.0001$; ICM: $F(1, 68) = 69.57$, $P < 0.0001$]. These findings suggest that HMGB1

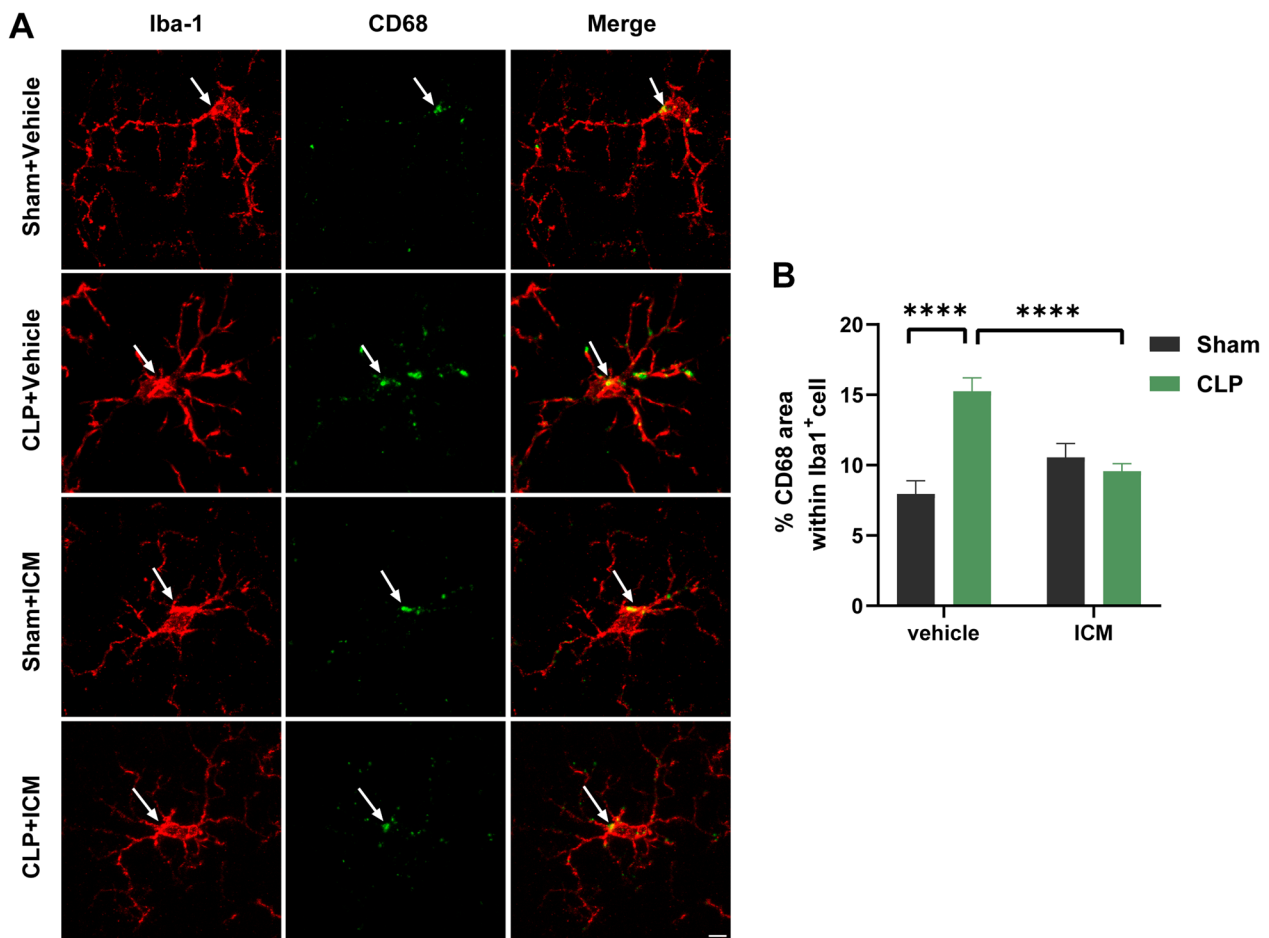


Fig. 4 ICM reversed the enhanced phagocytic activity of microglia in the hippocampus of SAE mice. **A** Representative images of immunofluorescence staining of CD68 (green) and Iba-1 (red) and colocalization in the hippocampus, scale bar = 5 μ m; **B** quantification of the percentage of CD68 area within Iba-1⁺ cells (microglia) in the hippocampus among the four groups. Data are presented as the mean \pm SEM (n = 4–6 mice/group). *****P* < 0.0001 vs. the indicated groups

mediates neuronal morphology damage and loss of dendritic spines.

ICM reversed the decreased theta oscillation in the hippocampus of SAE mice

We further evaluated the changes in neural oscillations in the hippocampus of SAE mice while the mice performed NOR. In the present study, the power of theta oscillation in the CLP + vehicle group was significantly decreased compared with that in the sham + vehicle group, and this effect was reversed by ICM treatment [Fig. 7D; interaction: CLP \times ICM, $F(1, 20) = 9.503$, $P = 0.0059$; CLP: $F(1, 20) = 1.198$, $P < 0.01$; ICM: $F(1, 20) = 9.623$, $P < 0.05$]. In addition, there were no significant differences in alpha, beta, and gamma oscillation power among the four groups [Fig. 7E; interaction: CLP \times ICM, $F(1, 20) = 0.9751$, $P = 0.3352$; CLP: $F(1, 20) = 0.06195$, $P = 0.1000$; ICM: $F(1, 20) = 6.120$, $P = 0.9527$; Fig. 7E;

interaction: CLP \times ICM, $F(1, 20) = 0.2811$, $P = 0.6018$; CLP: $F(1, 20) = 0.2811$, $P = 0.5929$; ICM: $F(1, 20) = 1.594$, $P = 0.8757$; Fig. 7G; interaction: CLP \times ICM, $F(1, 20) = 0.01186$, $P = 0.9144$; CLP: $F(1, 20) = 0.2811$, $P = 0.9894$; ICM: $F(1, 20) = 1.594$, $P = 0.9556$]. These results suggest that inhibiting HMGB1 reverses abnormal theta oscillation in the CA1 of the hippocampus after CLP.

ICM reversed the impairment of neuronal activity and synaptic dysfunction in the hippocampus of SAE mice

Given that neural oscillations are driven by fluctuations in the excitability of populations of neurons, we further examined neuronal activity in the hippocampus of SAE mice. C-Fos protein is the product of the immediate early gene that is a marker of neuronal activation (Morgan and Curran 1986; Dragunow

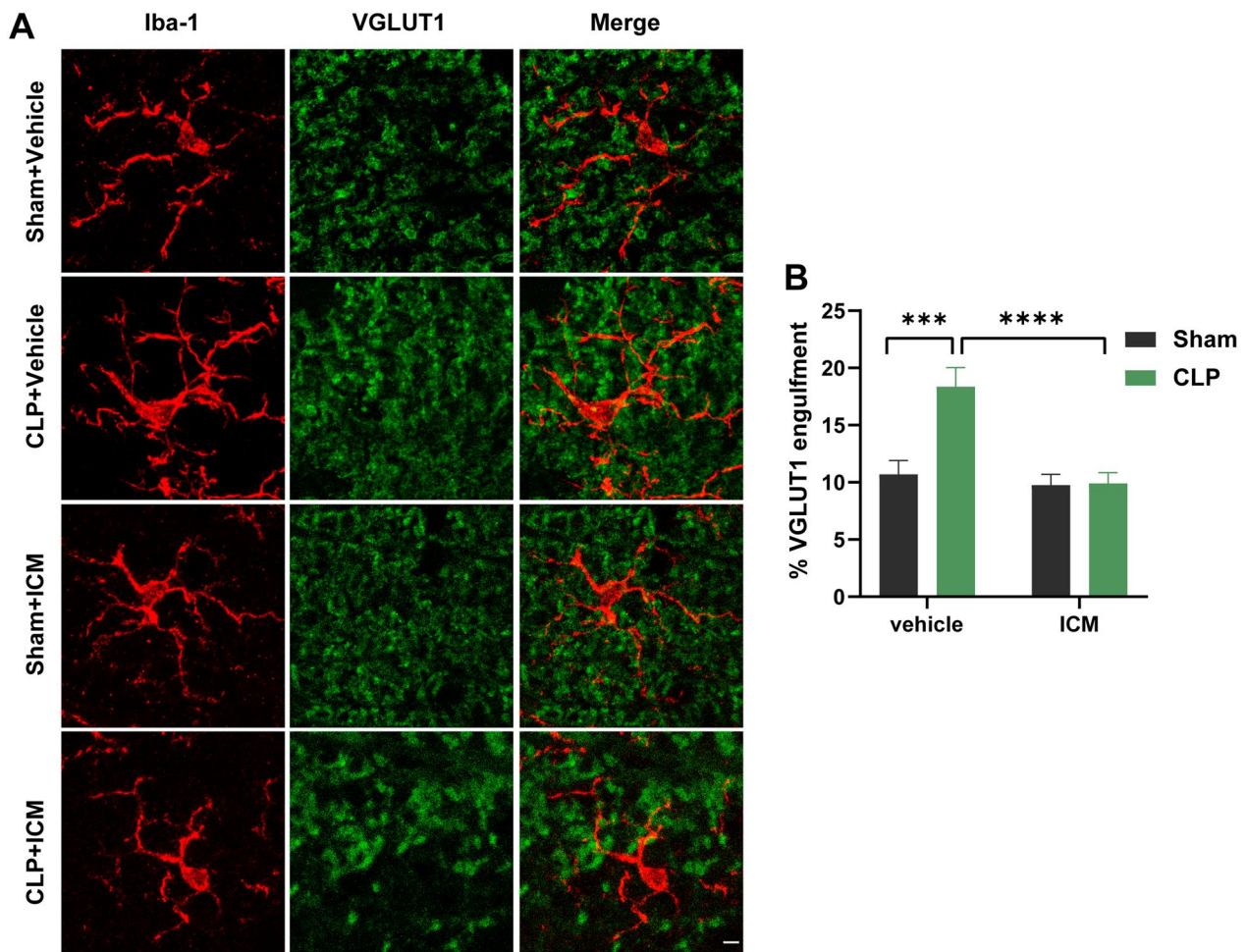


Fig. 5 ICM reduced microglial-mediated synapse elimination in the hippocampus of SAE mice. **A** Representative images of immunofluorescence staining of VGLUT1 (green), Iba-1 (red) and colocalization in the hippocampus, scale bar = 5 μ m; **B** quantification of the percentage of VGLUT1 engulfment within Iba-1⁺ cells (microglia) in the hippocampus among the four groups. Data are presented as the mean \pm SEM (n = 3–5 mice/group). *** P < 0.001 and **** P < 0.0001 vs. the indicated groups

and Faull 1989). The number of c-Fos⁺ cells in the CLP + vehicle group was significantly decreased compared with that in the sham + vehicle group, and ICM treatment reversed this effect [Fig. 8A, B; interaction: CLP \times ICM, $F(1, 68) = 20.56$, $P < 0.0001$; CLP: $F(1, 68) = 11.45$, $P < 0.0001$; ICM: $F(1, 68) = 5.935$, $P < 0.0001$]. Meanwhile, HFS-induced SC-CA1 LTP was significantly reduced in the hippocampus of the CLP + vehicle group compared with the sham + vehicle group, and this effect was also reversed by ICM

treatment [Fig. 8C–E; interaction: CLP \times ICM, $F(1, 17) = 1.560$, $P = 0.2287$; CLP: $F(1, 17) = 7.818$, $P < 0.01$; ICM: $F(1, 17) = 16.06$, $P < 0.05$]. These results suggest that HMGB1 impairs neuronal activity and synaptic function after CLP.

Discussion

In the present study, we showed that in SAE mice, HMGB1 mediates microglial activation and induces excessive phagocytosis of synapses and neuron

(See figure on next page.)

Fig. 6 ICM ameliorated abnormal neuronal morphology and loss of dendritic spines in the hippocampus of SAE mice. **A** Sholl analysis pattern map of neuronal morphology; **B** quantification of dendritic intersections of neuronal dendrites in the hippocampus among the four groups; **C** representative images of hippocampal neuronal tracings; **D** quantification of the number of neuronal branches in the hippocampus among the four groups; **E** quantification of the total length of neuronal branches in the hippocampus among the four groups; **F** representative images of the dendritic spines of hippocampal neurons; **G** quantification of dendritic spine density of neurons in the hippocampus among the four groups, scale bar = 10 μ m. Data are presented as the mean \pm SEM (n = 4 mice/group). **** P < 0.0001 vs. the indicated groups

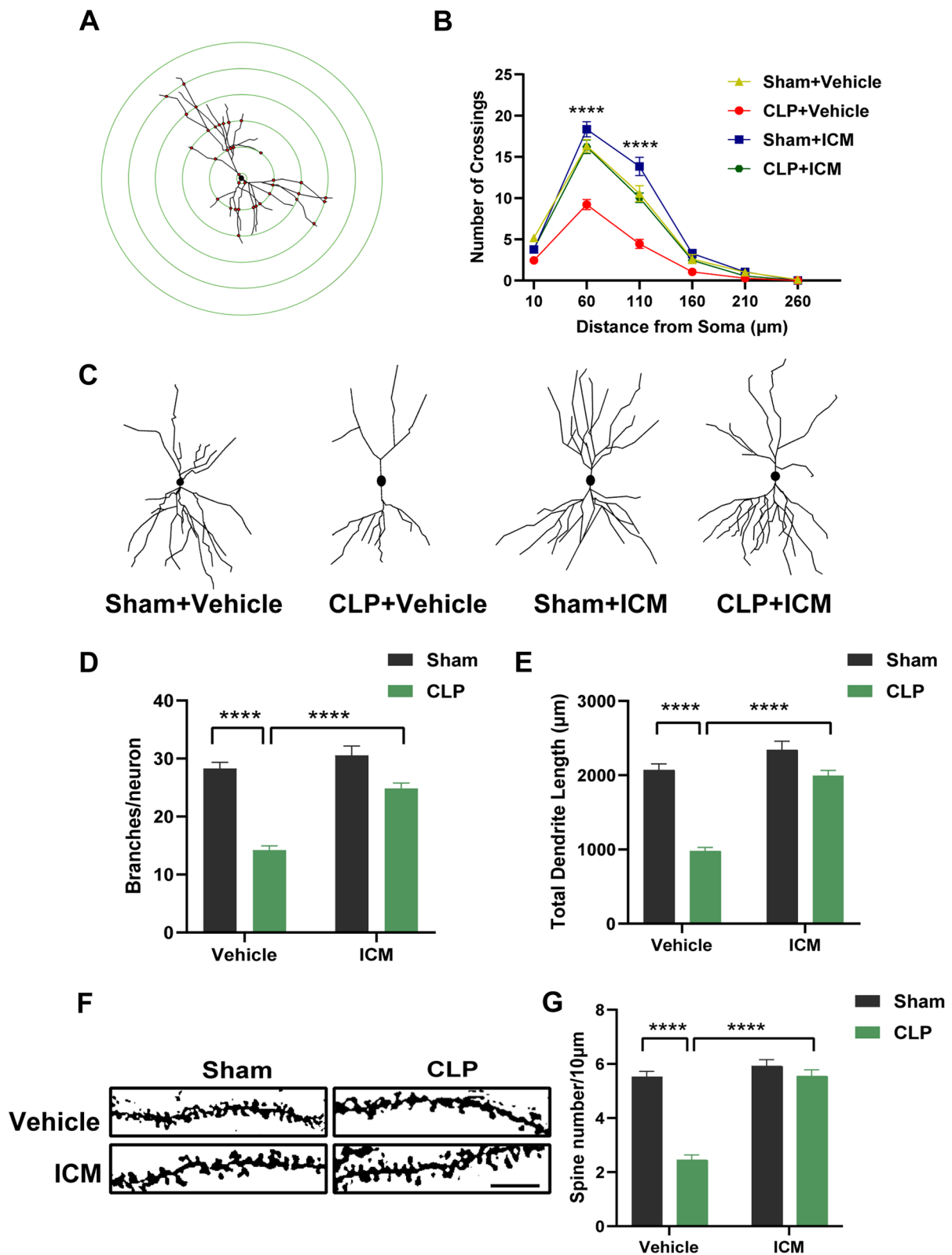


Fig. 6 (See legend on previous page.)

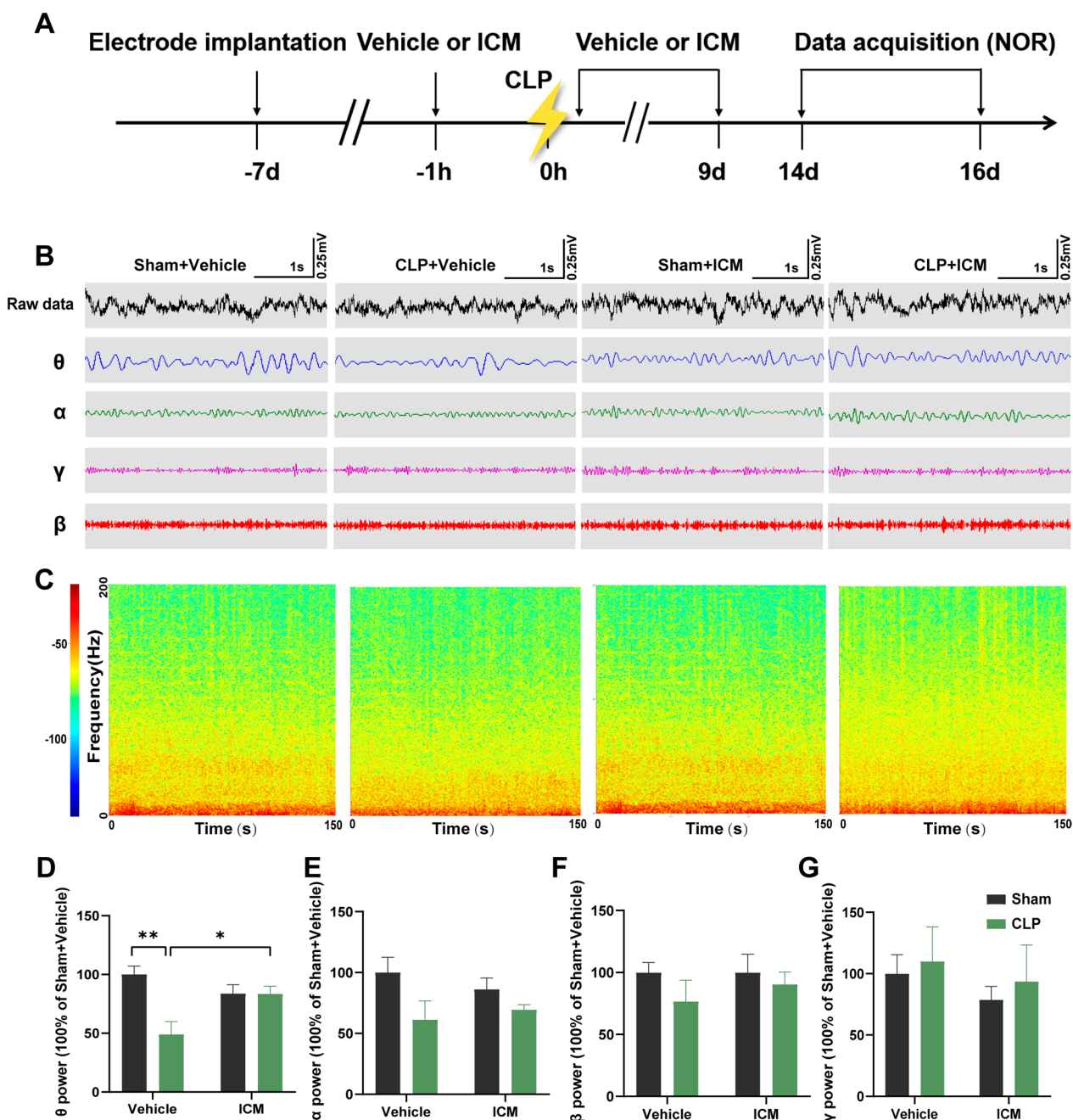


Fig. 7 ICM reversed the abnormal theta oscillation in the hippocampus of SAE mice. **A** Flow chart of the electrophysiological experiment. **B** Representative images of local field potential and filtered theta, alpha, beta, and gamma oscillations in the hippocampus among the four groups. **C** Example power spectra of local field potential in the hippocampus. **D–G** Quantification of average theta, alpha, beta, and gamma oscillation power in the hippocampus among the four groups. Data are shown as the mean \pm SEM ($n = 3–5$ mice/group), $*P < 0.05$ and $**P < 0.01$ vs. the indicated groups

dysfunction, ultimately leading to cognitive impairment. Notably, inhibiting HMGB1 secretion reverses these aberrant changes and ameliorates cognitive impairment in SAE mice (Fig. 9).

SAE is a severe CNS complication of sepsis, manifesting clinically as diffuse brain dysfunction, with varying degrees of neurological symptoms ranging from lethargy to coma, and over 80% of patients demonstrate EEG abnormalities [1, 24, 25]. SAE is the most common cause

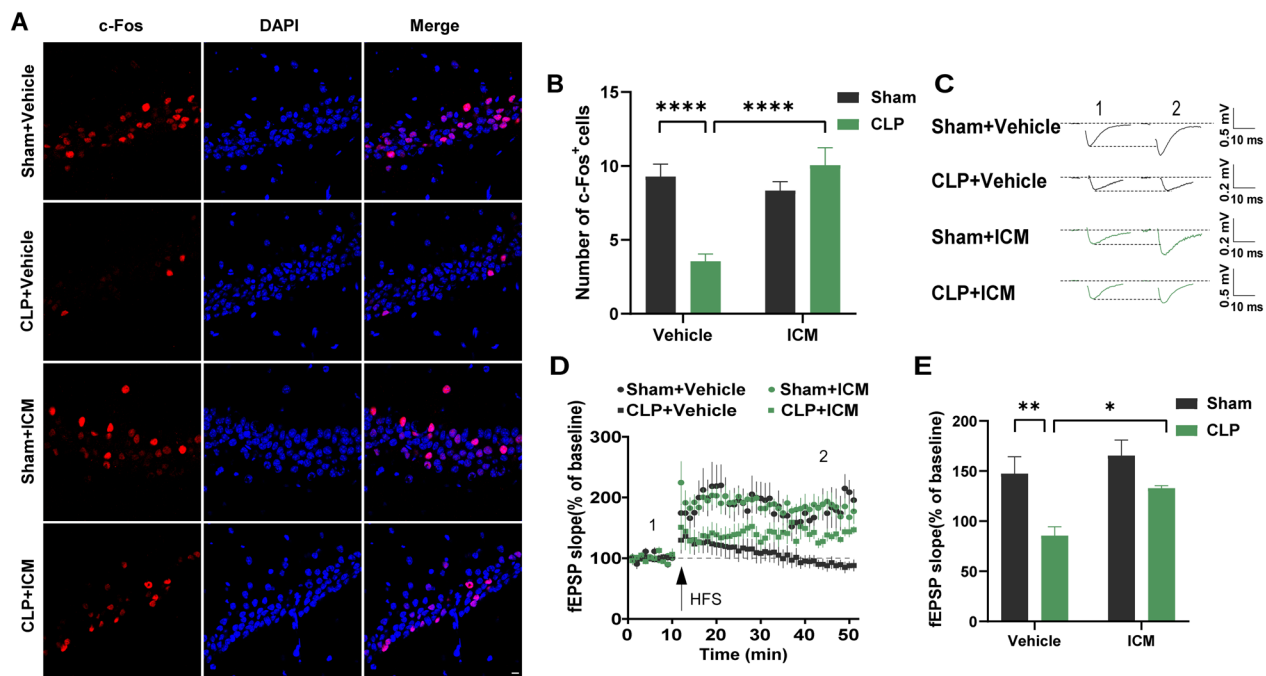


Fig. 8 ICM reversed the impairment of neuronal activity and synaptic dysfunction in the hippocampus of SAE mice. **A** Representative images of immunofluorescence staining of c-Fos (red), DAPI (blue) and colocalization in the hippocampus, scale bar = 10 μm; **B** quantification of the number of c-Fos⁺ cells in the hippocampus among the four groups. (n = 3 mice/group). **C** Schematic representation of fEPSPs before (1) and after (2) HFS among the four groups. Horizontal calibration bars, 10 ms; vertical bars, 0.5 mV. **D** Time-dependent changes in the slope of fEPSPs before (1) and after (2) HFS in hippocampal slices among the four groups. **E** Quantification of fEPSP slopes evoked by HFS among the four groups. (n = 5–6 slices/group). Data are presented as the mean ± SEM. **P* < 0.05, ***P* < 0.01, *****P* < 0.0001 vs. the indicated groups

of encephalopathy in medical and surgical intensive care [26], and approximately half (46%) of patients with sepsis have SAE [27]. After CLP, the surviving mice in our study exhibited impaired learning and memory, as assessed by the NOR and Y maze tests. Consistent with our results, it has been suggested that sepsis induced by CLP can lead to cognitive impairment [28]. Lipopolysaccharide (LPS) injection can also cause short- and long-term cognitive impairments through a mechanism that releases various inflammatory cytokines in the brain [29]. However, the CLP model induces a slower but more stable increase in plasma cytokines that resembles human sepsis more closely than endotoxin administration. The CLP model can also cause more prolonged and consistent cognitive impairment after sepsis relative to LPS administration. Therefore, CLP is considered the gold standard model for SAE [30].

The underlying pathological mechanisms of SAE are multifactorial and highly complex. BBB damage, cerebral microcirculation dysfunction, abnormal inflammatory response, and abnormal brain metabolism may all be involved in SAE development, but the specific mechanisms are not yet known [1]. Accumulating evidence suggests that neuroinflammation triggered by abnormal

inflammatory cytokine expression plays a pivotal role in SAE. It has been reported that activation of the NLRP3 inflammasome via mitophagy inhibition in cerebral microvascular endothelial cells may promote the secretion of IL-1β into the CNS and induce neuroinflammation, leading to SAE [5]. In addition, a previous study reported that double-stranded RNA dependent protein kinase could physically interact with inflammasome components and mediates inflammasome activation, thus regulating release of HMGB1 [31]. Interestingly, HMGB1 is also a late mediator of inflammation in sepsis [13] and participates in the amplification of neuroinflammation [32]. However, there are few studies on the role of HMGB1 in SAE. HMGB1 translocates from the nucleus into the cytoplasm and is eventually released into the extracellular space. The nucleus–cytoplasm transfer of HMGB1 is a critical step in the active release of HMGB1, decreasing n-HMGB1 levels [33, 34]. In our study, we demonstrated that the expression of n-HMGB1 was significantly decreased in the hippocampus after CLP, while ICM treatment inhibited HMGB1 secretion and reduced cognitive impairment. These results indicate that inhibiting HMGB1 secretion may be a critical potential mechanism for treating SAE. Consistent with our data, HMGB1

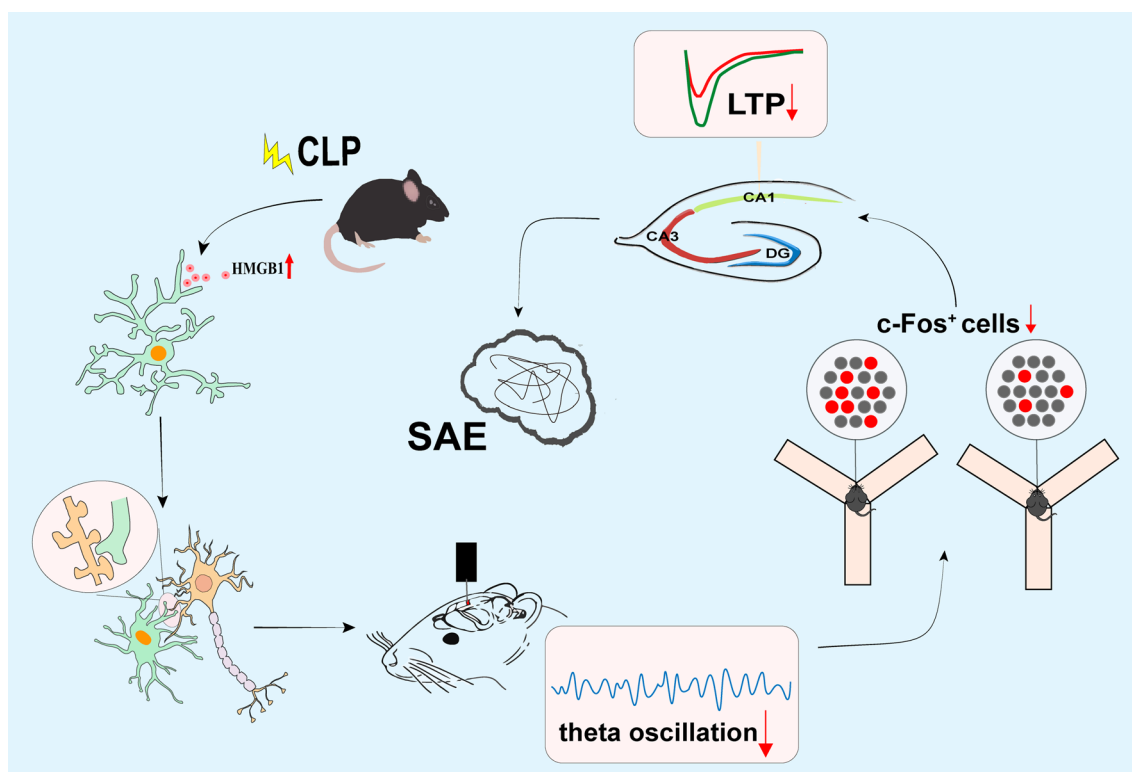


Fig. 9 The schematic diagram illustrates that CLP induces increased secretion of HMGB1 and microglial activation, thus causing abnormal synaptic elimination and decreased theta oscillation. Abnormal theta oscillation reduces c-Fos⁺ cells and impairs LTP, ultimately leading to cognitive impairment in SAE mice

release induces cognitive deficits in diabetes-related dementia and TBI [12, 35]. In an animal model of AD, HMGB1 induced cognitive impairment through the Sirtuin 3/superoxide dismutase 2 signaling pathway [11]. However, the mechanism by which HMGB1 induces cognitive impairment in SAE remains unclear.

Microglia are the primary immune cells in the brain and are the main source of cytokines in the CNS. Microglial activation induces a change from a resting state to a highly branched state (hyperramification), an increase in the average length of the branches and an amoebic state [36]. Our study showed that CLP increased the number and average length of microglial branches with a concomitant increased expression of CD68 in the hippocampus. These results suggest that the phagocytic ability of activated microglia is enhanced in SAE mice. Inhibiting HMGB1 secretion through ICM treatment reversed the above anomalies, suggesting that HMGB1 is a crucial factor in mediating microglial activation in SAE. Numerous studies have demonstrated that microglial activation is closely associated with cognitive impairment in AD, vascular dementia, postoperative cognitive impairment, cerebral ischemia-percussion injury, and TBI [37–40]. Additionally, under pathological conditions,

the enhanced phagocytic ability of long-term activated microglia can lead to excess inflammatory mediator expression, aberrant synaptic pruning, neuronal dysfunction, or even death [41]. In our study, excitatory synapses were engulfed by microglia following CLP, and this effect was rescued by ICM administration. These findings indicate that HMGB1 causes cognitive impairment by enhancing microglial phagocytic ability and inducing excitatory synaptic engulfment. However, a previous study suggested that GABA-receptive microglia selectively prune inhibitory synapses in postnatal development and impair this microglial response, leading to behavioral abnormalities such as attention-deficit/hyperactivity disorder [42]. The reasons for this discrepancy are unknown but may be due to the different animal models used.

In the CNS, neurons can process thousands of different synaptic inputs, with dendrites playing an essential role in the brain's neural network. Dendrites can receive input from other neurons, integrating and transmitting signals to the cell body, triggering the generation and propagation of neuronal action potentials, thus transferring information and performing complex cognitive tasks [43]. Dendritic spines are spiny protrusions of dendrites

and are the primary site of synaptic connections between neurons [44]. In this experiment, we examined changes in neuronal morphology and dendritic spine density of pyramidal neurons in the hippocampus by Golgi staining. We found that the neuronal morphology was impaired, and the dendritic spine density was significantly reduced after the CLP operation, suggesting that the synaptic structural integrity of the hippocampus in SAE mice was impaired. Inhibiting the secretion of HMGB1 improved the abnormal morphological changes in pyramidal neurons and the loss of dendritic spines in the hippocampus of SAE mice. Conversely, HMGB1 can promote neurite outgrowth and cell migration during early brain development and is essential for processes such as forebrain development [45]. This discrepancy is most likely due to the different redox state of HMGB1 which resulting in activation of different HMGB1 receptors and subsequent biological outcome [46]. The release of all-thiol (all-reduced) HMGB1 potentiates chemotaxis and promotes neurite outgrowth via binding to receptor for advanced glycation end products. During inflammation, the disulfide form of HGMB1 releasing from activated macrophage binds to Toll-like receptor 4 to induce cytokine production [46–48]. In addition, a disintegrin and metalloproteinase domain 10 is involved in dendritic spine shaping in an animal model of AD, which alters dendritic morphology, induces dendritic spine loss, and impairs information transfer between neurons [49]. Dendritic spines are essential for receiving neurotransmitters and regulating synaptic plasticity, which is the basis of learning and memory [50]. Activated microglia cause dendritic spine loss and neuronal damage or death by increasing synaptic phagocytosis, which can cause various neuropsychiatric disorders [51–53]. These results suggest a complex interaction between microglia and neurons under different conditions, promoting the formation of neuronal connections and maintaining an optimal neural network.

Neural oscillations are the rhythms of neural activity observed at different temporal and spatial scales, which are classified as delta oscillations (1–4 Hz), theta oscillations (4–8 Hz), alpha oscillations (8–12 Hz), beta oscillations (12–30 Hz) and gamma oscillations (30–90 Hz) [54]. Numerous studies have shown that neural oscillations play vital roles in perceptual, cognitive, motor, and emotional processes [55]. For example, in animal models of schizophrenia, diminished gamma oscillations have been shown to lead to impaired cognitive function [56, 57]. We detected neural oscillations of the hippocampus in mice performing NOR to further investigate the neural mechanisms underlying cognitive impairment in SAE. Interestingly, our study indicated that theta oscillation power was significantly decreased after CLP, and

this effect was reversed by ICM treatment. In an animal model of AD, inhibitory and rhythmic septohippocampal activity are selectively reduced, and hippocampal theta oscillation power is impaired during a cognitive task, leading to behavioral disorders in information processing [58]. In addition, several intracranial studies have suggested that increased theta power is associated with successful encoding or retrieval [59, 60]. A previous study demonstrated that the reduction in LFP cross-frequency coupling between theta and gamma power in the hippocampus is associated with impaired LTP in an animal model of transient global cerebral ischemia [61]. Consistently, our study indicated that decreased theta oscillation was accompanied by reduced activity of neurons and impaired LTP in the hippocampus of SAE mice. These results suggest that HMGB1 mediates theta oscillation disruption and network dysregulation, thus leading to cognitive deficits in SAE.

Conclusions

Our study demonstrated that increased HMGB1 secretion induces microglial activation, which in turn induces abnormal synaptic elimination and neuronal dysfunction in the hippocampus, ultimately leading to cognitive impairments in SAE mice. Administration of ICM effectively alleviated these pathological changes and sepsis-induced cognitive impairment. Our study suggests that HMGB1 may be a target for the treatment of SAE.

Abbreviations

SAE	Sepsis-associated encephalopathy
HMGB1	High mobility group box-1 protein
CLP	Cecal ligation and puncture
ICM	Inflachromene
LTP	Long-term potentiation
CNS	Central nervous system
EEG	Electroencephalography
BBB	Blood–brain barrier
AD	Alzheimer's disease
TBI	Traumatic brain injury
OFT	Open field test
NOR	Novel object recognition test
ACSF	Artificial cerebrospinal fluid
SC	Schaffer collateral
HFS	High-frequency stimulation
LPS	Lipopolysaccharide

Acknowledgements

The authors would like to thank the MARC of Nanjing University and the staff for providing animal care during this study.

Author contributions

YYY and XHT designed this work. YYY wrote the paper. YYY, XHT, and SXW performed the experiments. YYY, YCZ and MJ analyzed the data. JCS, MHJ and JJY directed the discussion. All authors read and approved the final manuscript.

Funding

This study was supported by grants from the National Natural Science Foundation of China (to JJY, No. 81971020).

Availability of data and materials

The datasets used and/or analysed during the current study are available from the corresponding author on reasonable request.

Declarations**Ethics approval and consent to participate**

All animal experiments and related operations were carried out in accordance with the Guideline for the Care and Use of Laboratory Animals from the Animal Center of Jinling Hospital and the National Institutes of Health.

Consent for publication

Not applicable.

Competing interests

The authors declare that they have no competing interests.

Author details

¹Department of Anesthesiology, Jinling Hospital, Medical School of Nanjing University, Nanjing 210002, China. ²Department of Anesthesiology, Pain and Perioperative Medicine, The First Affiliated Hospital of Zhengzhou University, Zhengzhou 450000, China. ³Department of Anesthesiology, The Second Affiliated Hospital, Nanjing Medical University, Nanjing 210011, China.

Received: 8 December 2022 Accepted: 2 March 2023

Published online: 11 March 2023

References

- Gofton TE, Young GB. Sepsis-associated encephalopathy. *Nat Rev Neurol*. 2012;8:557–66.
- Di Bella D, Ferreira JPS, Silva RNO, Echem C, Milan A, Akamine EH, Carvalho MH, Rodrigues SF. Gold nanoparticles reduce inflammation in cerebral microvessels of mice with sepsis. *J Nanobiotechnol*. 2021;19:52.
- Manabe T, Heneka MT. Cerebral dysfunctions caused by sepsis during ageing. *Nat Rev Immunol*. 2021;22(7):444–58.
- Zhang Y, Chen S, Tian W, Zhu H, Li W, Dai W, Zhang X, Gu X, Su D. Emerging trends and hot spots in sepsis-associated encephalopathy research from 2001 to 2021: a bibliometric analysis. *Front Med (Lausanne)*. 2022;9:817351.
- Ding H, Li Y, Chen S, Wen Y, Zhang S, Luo E, Li X, Zhong W, Zeng H. Fisetin ameliorates cognitive impairment by activating mitophagy and suppressing neuroinflammation in rats with sepsis-associated encephalopathy. *CNS Neurosci Ther*. 2022;28:247–58.
- Poles MZ, Naszai A, Gulacsi L, Czako BL, Gal KG, Glenz RJ, Dookhun D, Rutai A, Tallosy SP, Szabo A, et al. Kynurenic acid and its synthetic derivatives protect against sepsis-associated neutrophil activation and brain mitochondrial dysfunction in rats. *Front Immunol*. 2021;12:717157.
- Moraes CA, Zaverucha-do-Valle C, Fleurance R, Sharshar T, Bozza FA, d'Avila JC. Neuroinflammation in sepsis: molecular pathways of microglia activation. *Pharmaceuticals (Basel)*. 2021;14:416.
- Wang H, Bloom O, Zhang M, Vishnubhakat JM, Ombrellino M, Che J, Frazier A, Yang H, Ivanova S, Borovikova L, et al. HMG-1 as a late mediator of endotoxin lethality in mice. *Science*. 1999;285:248–51.
- Andersson U, Tracey KJ. HMGB1 is a therapeutic target for sterile inflammation and infection. *Annu Rev Immunol*. 2011;29:139–62.
- Zhang Z, Jiang J, He Y, Cai J, Xie J, Wu M, Xing M, Zhang Z, Chang H, Yu P, et al. Pregabalin mitigates microglial activation and neuronal injury by inhibiting HMGB1 signaling pathway in radiation-induced brain injury. *J Neuroinflamm*. 2022;19:231.
- Gao J-M, Zhang X, Shu G-T, Chen N-N, Zhang J-Y, Xu F, Li F, Liu Y-G, Wei Y, He Y-Q, et al. Trilobatin rescues cognitive impairment of Alzheimer's disease by targeting HMGB1 through mediating SIRT3/SOD2 signaling pathway. *Acta Pharmacol Sin*. 2022;43(10):2482–94.
- Tan SW, Zhao Y, Li P, Ning YL, Huang ZZ, Yang N, Liu D, Zhou YG. HMGB1 mediates cognitive impairment caused by the NLRP3 inflammasome in the late stage of traumatic brain injury. *J Neuroinflamm*. 2021;18:241.
- Sunden-Cullberg J, Norrby-Teglund A, Rouhiainen A, Rauvala H, Herman G, Tracey KJ, Lee ML, Andersson J, Tokics L, Treutiger CJ. Persistent elevation of high mobility group box-1 protein (HMGB1) in patients with severe sepsis and septic shock. *Crit Care Med*. 2005;33:564–73.
- Zhuang X, Yu Y, Jiang Y, Zhao S, Wang Y, Su L, Xie K, Yu Y, Lu Y, Lv G. Molecular hydrogen attenuates sepsis-induced neuroinflammation through regulation of microglia polarization through an mTOR-autophagy-dependent pathway. *Int Immunopharmacol*. 2020;81:106287.
- Chavan SS, Huerta PT, Robbiati S, Valdes-Ferrer SI, Ochani M, Dancho M, Frankfurt M, Volpe BT, Tracey KJ, Diamond B. HMGB1 mediates cognitive impairment in sepsis survivors. *Mol Med*. 2012;18:930–7.
- Lee S, Nam Y, Koo JY, Lim D, Park J, Ock J, Kim J, Suk K, Park SB. A small molecule binding HMGB1 and HMGB2 inhibits microglia-mediated neuroinflammation. *Nat Chem Biol*. 2014;10:1055–60.
- Iachettini S, Ciccarone F, Maresca C, D'Angelo C, Petti E, Di Vito S, Ciriolo MR, Zizza P, Biroccio A. The telomeric protein TERF2/TRF2 impairs HMGB1-driven autophagy. *Autophagy*. 2022. <https://doi.org/10.1080/15548627.2022.2138687>.
- Li F, Huangyang P, Burrows M, Guo K, Riscal R, Godfrey J, Lee KE, Lin N, Lee P, Blair IA, et al. FBP1 loss disrupts liver metabolism and promotes tumorigenesis through a hepatic stellate cell senescence secretome. *Nat Cell Biol*. 2020;22:728–39.
- Borst K, Dumas AA, Prinz M. Microglia: immune and non-immune functions. *Immunity*. 2021;54:2194–208.
- David S, Kroner A. Repertoire of microglial and macrophage responses after spinal cord injury. *Nat Rev Neurosci*. 2011;12:388–99.
- Wang C, Yue H, Hu Z, Shen Y, Ma J, Li J, Wang XD, Wang L, Sun B, Shi P, et al. Microglia mediate forgetting via complement-dependent synaptic elimination. *Science*. 2020;367:688–94.
- Cho W, Koo JY, Park Y, Oh K, Lee S, Song JS, Bae MA, Lim D, Lee DS, Park SB. Treatment of sepsis pathogenesis with high mobility group box protein 1-regulating anti-inflammatory agents. *J Med Chem*. 2017;60:170–9.
- Li Z, Vidjro OE, Guo G, Du Y, Zhou Y, Xie Q, Li J, Gao K, Zhou L, Ma T. NLRP3 deficiency decreases alcohol intake controlling anxiety-like behavior via modification of glutamatergic transmission in corticostriatal circuits. *J Neuroinflamm*. 2022;19:308.
- Peidaee E, Sheybani F, Naderi H, Khosravi N, Jabbari NM. The etiological spectrum of febrile encephalopathy in adult patients: a cross-sectional study from a developing country. *Emerg Med Int*. 2018;2018:3587014.
- Schuler A, Wulf DA, Lu Y, Iwashyna TJ, Escobar GJ, Shah NH, Liu VX. The impact of acute organ dysfunction on long-term survival in sepsis. *Crit Care Med*. 2018;46:843–9.
- Bleck TP, Smith MC, Pierre-Louis SJ, Jares JJ, Murray J, Hansen CA. Neurologic complications of critical medical illnesses. *Crit Care Med*. 1993;21:98–103.
- Bolton CF, Young GB, Zochodne DW. The neurological complications of sepsis. *Ann Neurol*. 1993;33:94–100.
- Savi FF, de Oliveira A, de Medeiros GF, Bozza FA, Michels M, Sharshar T, Dal-Pizzol F, Ritter C. What animal models can tell us about long-term cognitive dysfunction following sepsis: a systematic review. *Neurosci Biobehav Rev*. 2021;124:386–404.
- Czerniawski J, Miyashita T, Lewandowski G, Guzowski JF. Systemic lipopolysaccharide administration impairs retrieval of context-object discrimination, but not spatial, memory: evidence for selective disruption of specific hippocampus-dependent memory functions during acute neuroinflammation. *Brain Behav Immun*. 2015;44:159–66.
- Dejager L, Pinheiro I, Dejonckheere E, Libert C. Cecal ligation and puncture: the gold standard model for polymicrobial sepsis? *Trends Microbiol*. 2011;19:198–208.
- Lu B, Nakamura T, Inouye K, Li J, Tang Y, Lundback P, Valdes-Ferrer SI, Olofsson PS, Kalb T, Roth J, et al. Novel role of PKR in inflammasome activation and HMGB1 release. *Nature*. 2012;488:670–4.
- Frank MG, Weber MD, Watkins LR, Maier SF. Stress sounds the alarm: the role of the danger-associated molecular pattern HMGB1 in stress-induced neuroinflammatory priming. *Brain Behav Immun*. 2015;48:1–7.
- Franklin TC, Wohleb ES, Zhang Y, Fogaça M, Hare B, Duman RS. Persistent increase in microglial RAGE contributes to chronic stress-induced priming of depressive-like behavior. *Biol Psychiatry*. 2018;83:50–60.
- Wang B, Huang X, Pan X, Zhang T, Hou C, Su WJ, Liu LL, Li JM, Wang YX. Minocycline prevents the depressive-like behavior through inhibiting the release of HMGB1 from microglia and neurons. *Brain Behav Immun*. 2020;88:132–43.

35. Jeong JH, Lee DH, Song J. HMGB1 signaling pathway in diabetes-related dementia: blood–brain barrier breakdown, brain insulin resistance, and A β accumulation. *Biomed Pharmacother.* 2022;150: 112933.
36. Walker FR, Beynon SB, Jones KA, Zhao Z, Kongsui R, Cairns M, Nilsson M. Dynamic structural remodelling of microglia in health and disease: a review of the models, the signals and the mechanisms. *Brain Behav Immun.* 2014;37:1–14.
37. Xiang X, Tang X, Yu Y, Xie S, Liu L, Chen M, Zhang R, Kang X, Zheng Y, Yang G, et al. Role of lipocalin-2 in surgery-induced cognitive decline in mice: a signal from neuron to microglia. *J Neuroinflamm.* 2022;19:92.
38. Yi-Bin W, Xiang L, Bing Y, Qi Z, Fei-Tong J, Minghong W, Xiangxiang Z, Le K, Yan L, Ping S, et al. Inhibition of the CEBP β -NF κ B interaction by nanocarrier-packaged carnosic acid ameliorates glia-mediated neuroinflammation and improves cognitive function in an Alzheimer's disease model. *Cell Death Dis.* 2022;13:318.
39. Xia Q, Zhan G, Mao M, Zhao Y, Li X. TRIM45 causes neuronal damage by aggravating microglia-mediated neuroinflammation upon cerebral ischemia and reperfusion injury. *Exp Mol Med.* 2022;54:180–93.
40. Zheng P, Bai Q, Feng J, Zhao B, Duan J, Zhao L, Liu N, Ren D, Zou S, Chen W. Neonatal microglia and proteinase inhibitors-treated adult microglia improve traumatic brain injury in rats by resolving the neuroinflammation. *Bioeng Transl Med.* 2022;7: e10249.
41. Choi I, Heaton GR, Lee YK, Yue Z. Regulation of α -synuclein homeostasis and inflammasome activation by microglial autophagy. *Sci Adv.* 2022;8: eabn1298.
42. Favuzzi E, Huang S, Saldi GA, Binan L, Ibrahim LA, Fernández-Otero M, Cao Y, Zeine A, Sefah A, Zheng K, et al. GABA-receptive microglia selectively sculpt developing inhibitory circuits. *Cell.* 2021;184:4048–4063.e4032.
43. Beaulieu-Laroche L, Toloza EHS, Brown NJ, Harnett MT. Widespread and highly correlated somato-dendritic activity in cortical layer 5 neurons. *Neuron.* 2019;103:235–241.e234.
44. Helm MS, Dankovich TM, Mandad S, Rammner B, Jähne S, Salimi V, Koerbs C, Leibbrandt R, Urlaub H, Schikorski T, Rizzoli SO. A large-scale nanoscopy and biochemistry analysis of postsynaptic dendritic spines. *Nat Neurosci.* 2021;24:1151–62.
45. Fang P, Schachner M, Shen YQ. HMGB1 in development and diseases of the central nervous system. *Mol Neurobiol.* 2012;45:499–506.
46. Chen JQ, Gao SQ, Luo L, Jiang ZY, Liang CF, He HY, Guo Y. Nonoxid-HMGB1 attenuates cognitive impairment after traumatic brain injury in rats. *Front Med (Lausanne).* 2022;9: 827585.
47. Agalave NM, Svensson CI. Extracellular high-mobility group box 1 protein (HMGB1) as a mediator of persistent pain. *Mol Med.* 2015;20:569–78.
48. Huttunen HJ, Kuja-Panula J, Sorci G, Agneletti AL, Donato R, Rauvala H. Coregulation of neurite outgrowth and cell survival by amphoterin and S100 proteins through receptor for advanced glycation end products (RAGE) activation. *J Biol Chem.* 2000;275:40096–105.
49. Musardo S, Therin S, Pelucchi S, D'Andrea L, Stringhi R, Ribeiro A, Manca A, Balducci C, Pagano J, Sala C, et al. The development of ADAM10 endocytosis inhibitors for the treatment of Alzheimer's disease. *Mol Ther.* 2022;30(7):2474–90.
50. Cornejo VH, Ofer N, Yuste R. Voltage compartmentalization in dendritic spines in vivo. *Science.* 2022;375:82–6.
51. Nguyen PT, Dorman LC, Pan S, Vainchtein ID, Han RT, Nakao-Inoue H, Taloma SE, Barron JJ, Molofsky AB, Kheirbek MA, Molofsky AV. Microglial remodeling of the extracellular matrix promotes synapse plasticity. *Cell.* 2020;182:388–403.e315.
52. Sheridan SD, Horng JE, Perlis RH. Patient-derived in vitro models of microglial function and synaptic engulfment in schizophrenia. *Biol Psychiatry.* 2022;92(6):470–9.
53. Xie Z, Meng J, Wu Z, Nakanishi H, Hayashi Y, Kong W, Lan F, Narengaowa, Yang Q, Qing H, Ni J. The dual nature of microglia in Alzheimer's disease: a microglia-neuron crosstalk perspective. *Neuroscientist.* 2022. <https://doi.org/10.1177/10738584211070273>.
54. Cole SR, Voytek B. Brain oscillations and the importance of waveform shape. *Trends Cogn Sci.* 2017;21:137–49.
55. Siegel M, Donner TH, Engel AK. Spectral fingerprints of large-scale neuronal interactions. *Nat Rev Neurosci.* 2012;13:121–34.
56. Enomoto T, Tse MT, Floresco SB. Reducing prefrontal gamma-aminobutyric acid activity induces cognitive, behavioral, and dopaminergic abnormalities that resemble schizophrenia. *Biol Psychiatry.* 2011;69:432–41.
57. Lodge DJ, Behrens MM, Grace AA. A loss of parvalbumin-containing interneurons is associated with diminished oscillatory activity in an animal model of schizophrenia. *J Neurosci.* 2009;29:2344–54.
58. Villette V, Poindessous-Jazat F, Simon A, Léna C, Roullot E, Bellesort B, Epelbaum J, Dutar P, Stéphan A. Decreased rhythmic GABAergic septal activity and memory-associated theta oscillations after hippocampal amyloid-beta pathology in the rat. *J Neurosci.* 2010;30:10991–1003.
59. Solomon EA, Lega BC, Sperling MR, Kahana MJ. Hippocampal theta codes for distances in semantic and temporal spaces. *Proc Natl Acad Sci USA.* 2019;116:24343–52.
60. Herweg NA, Sharan AD, Sperling MR, Brandt A, Schulze-Bonhage A, Kahana MJ. Reactivated spatial context guides episodic recall. *J Neurosci.* 2020;40:2119–28.
61. Zheng L, Yu M, Lin R, Wang Y, Zhuo Z, Cheng N, Wang M, Tang Y, Wang L, Hou ST. Rhythmic light flicker rescues hippocampal low gamma and protects ischemic neurons by enhancing presynaptic plasticity. *Nat Commun.* 2020;11:3012.

Publisher's Note

Springer Nature remains neutral with regard to jurisdictional claims in published maps and institutional affiliations.

Ready to submit your research? Choose BMC and benefit from:

- fast, convenient online submission
- thorough peer review by experienced researchers in your field
- rapid publication on acceptance
- support for research data, including large and complex data types
- gold Open Access which fosters wider collaboration and increased citations
- maximum visibility for your research: over 100M website views per year

At BMC, research is always in progress.

Learn more biomedcentral.com/submissions

